Parameter sensitivity of a MRAS-based sensorless control for AFPMSM considering speed accuracy and dynamic response at multiple parameter variations

Michael Brüns, Christian Rudolph, Tankred Müller
Hamburg University of Applied Sciences
Faculty of Engineering and Computer Science
Berliner Tor 21
Hamburg, Germany
Michael.Bruens@haw-hamburg.de; Christian.Rudolph@haw-hamburg.de;
Tankred.Mueller@haw-hamburg.de

Keywords

Sensorless control, Axial flux machines, Permanent magnet motor, Optimal control, Optimization method, Speed control, System identification, Real-time processing.

Abstract

In this paper, a novel approach is presented to tune the sensorless control based on a model reference adaptive system method (MRAS-based) in order to balance the variation of several system parameters. The method was used for speed and position estimation of a field-oriented controlled (FOC) wheel hub drive with an axial flux permanent magnet synchronous motor (AFPMSM). Parameter deviations of the control system are assumed to occur as disturbances. Their influences are reduced using an enhanced fundamental wave model of the AFPMSM. A model-based system engineering (MBSE) approach was chosen to compare simulation with experimental results. Following the simulation study, the MRAS-based method was implemented on a target system directly from the simulation models using code generation software. A performance evaluation of the tuning algorithm is focused on the accuracy of the calculated rotor position. The results demonstrate a resource-efficient MRAS implementation on a microcontroller (µC) suitable for operation with multiple parameter variations.

1 Introduction

The permanent magnet synchronous motor (PMSM) is a popular machine for modern drive solutions. It meets the requirements for high power density, high efficiency and sufficient robustness in the fields of mobile machinery, electromobility or some industrial applications at attractive system costs. But some drives require a particularly elevated energy density in addition of a short axial length. Therefore the choice of an AFPMSM could provide further advantages [1]-[2]. This type of permanent magnet synchronous machine is characterized by a design in which the air gap field is oriented axially, i.e. in the direction of the shaft, s. Fig. 1. Moreover, the machine can be extended using a modular design, for example as single stator double rotor or double stator, single rotor versions. The AFPMSM configuration enables a flat, cylindrical construction shape, which is ideal for integration as a wheel hub drive. However, the AFPMSM can be described by the same fundamental wave model as the PMSM.
Furthermore, sensorless control strategies are advantageous due to system simplifications increasing the reliability, reducing construction space and service costs of the drive system. Above all the redundant evaluation of a safety-critical system path becomes possible. In practice there are two main categories of sensorless control schemes subdivided in model-based sensorless control techniques for the medium and high-speed range and the saliency-based methods addressing the low speed range [3]. The MRAS-based speed estimators belong to the model-based group and present a closed loop method. Due to their advantages, such as straight forward design and comparative easy implementation on a µC they are recommended for low-cost applications, but can also be used in complex applications utilizing additional extensions [4]. Disadvantageous is the sensitivity on parameter variations of the real system, which can be reduced by an implementation of an optional parameter identification strategy [5]. Some publications release studies on the influence of parameters variations for the MRAS-based method by

simulation changing particular parameters[6], [7]. However, in practice there are different parameter uncertainties at once. Therefore, this research focuses on the comparison of simulation and experimental results to identify an option to optimize the method under multiple parameter variations in order to increase the performance in practice.

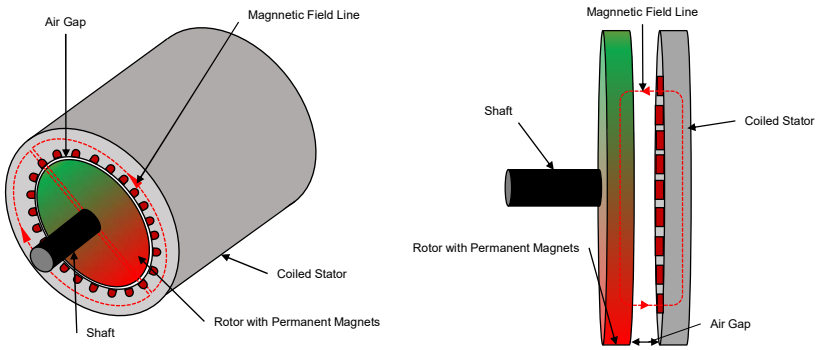

(a) (b)

Fig. 1: Comparison of an interior-rotor PMSM and the AFPMSM:
a) structure of a radial flux permanent magnet synchronous motor with two poles
b) structure of an axial flux permanent magnet synchronous motor with single stator and single rotor design, two-poles

2 MRAS-based sensorless control method

The MRAS method for speed and position estimation is based on the comparison of two independent machine models. Its adaptation mechanism is fed by the difference between state variables of the reference and the adjustable model. In the investigated MRAS-based method, the controlled machine itself serves as reference system and the measured stator current is used to adjust the model [4]. This creates a structure similar to an adaptive observer, but without the observer gain matrix as illustrated in Fig. 2.

The chosen method to design the adaptation mechanism is crucial for the stability of the sensorless control. There are three basic approaches [6]. One method is based on a local parameter optimization theory, missing sufficient stability conditions for operating in a wide field. A second method relies on the Lyapunov function and the third method is the one studied in this paper, based on the hyperstability theory design by V. M. Popov. There are indications that in practical systems the approach by Popov is superior in terms of response speed and convergence speed, since it yields a PI structure in contrast to a pure integral structure using the Lyapunov function [8]. However, both theories give a concept for sector stability of nonlinear feedback systems.

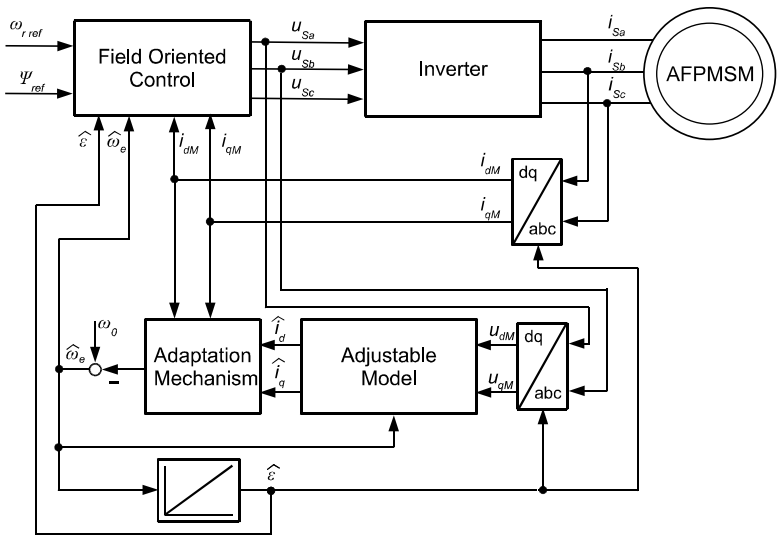

Fig. 2: MRAS-based sensorless control structure for an AFPMSM

2.1 Reference AFPMSM-model

The reference model can be described using the stator voltage equation of the AFPMSM. This is the well-known fundamental wave model [9] with the EMF induced by the permanent magnets, assuming a symmetrical winding distribution, neglecting saturation effects. Focused on machine parameter variation, it has to be considered which parts of the reference model can be imprecise. The machine parameters are dependent on the operating points, but in this approach, they are a part of the reference system, so they can be set as fixed. This includes the real values of the stator inductances L_d and L_q, the stator resistance R_s, the rotor magnetic flux Ψ_{PM}, the electrical rotation speed ω_e, the mechanical rotor speed ω, the flux-oriented angle ε, the number of pole pairs p and the stator currents and voltages i_d, i_q and u_d, u_q. However, the information we obtain about currents, voltages and the field or rotor angle by measurement and calculation are subject of errors in general, which are considered using error elements Δx_x. For example, the measured current consists of its actual real value and an unknown absolute error as follows:

$$\begin{bmatrix} i_{dM} \\ i_{qM} \end{bmatrix} = \begin{bmatrix} i_d \\ i_q \end{bmatrix} + \begin{bmatrix} \Delta i_d \\ \Delta i_q \end{bmatrix} \tag{1}$$

Subsequently, in the mathematical description of the reference AFPMSM-model these uncertainties are taken into account:

$$\begin{bmatrix} \frac{di_{dM}}{dt} \\ \frac{di_{qM}}{dt} \end{bmatrix} = \begin{bmatrix} -\frac{R_s}{L_d} & \omega_e * \frac{L_q}{L_d} \\ -\omega_e * \frac{L_d}{L_q} & -\frac{R_s}{L_q} \end{bmatrix} \begin{bmatrix} i_{dM} \\ i_{qM} \end{bmatrix} + \begin{bmatrix} \frac{1}{L_d} & 0 \\ 0 & \frac{1}{L_q} \end{bmatrix} \begin{bmatrix} u_{dM} \\ u_{qM} \end{bmatrix} + \begin{bmatrix} \frac{\Psi_{PM}}{L_q} \cdot sin(\Delta\epsilon) \\ -\frac{\Psi_{PM}}{L_q} \cdot cos(\Delta\epsilon) \end{bmatrix} \cdot \omega_e \tag{2}$$

2.2 Novel adjustable AFPMSM model approach considering parameter variation

The adjustable model is established in a similar way as the reference model, i.e. a fundamental wave model. Calculated or adjusted parameters of the adjustable model are indicated by the circumflex. Parameter deviations are taken into account using the theory of error. E.g. the stator resistance R_{sM} is described by its real value and an absolute error:

$$R_{sM} = R_s + \Delta R_s \tag{3}$$

Furthermore, an enhancement of the fundamental wave model using tuning parameters labeled $\hat{z}_d$ and $\hat{z}_q$ will be discussed. The mathematical description of the adjusted AFPMSM-model therefore includes influences by model parameter uncertainties and two tuning parameters $\hat{z}_d$ and $\hat{z}_q$:

$$\begin{bmatrix} \frac{d\hat{i}_d}{dt} \\ \frac{d\hat{i}_q}{dt} \end{bmatrix} = \begin{bmatrix} -\frac{R_{sM}}{L_{dM}} & \hat{\omega}_e \cdot \frac{L_{qM}}{L_{dM}} \\ -\hat{\omega}_e \cdot \frac{L_{dM}}{L_{qM}} & -\frac{R_{sM}}{L_{qM}} \end{bmatrix} \begin{bmatrix} \hat{i}_d \\ \hat{i}_q \end{bmatrix} + \begin{bmatrix} \frac{1}{L_{dM}} & 0 \\ 0 & \frac{1}{L_{qM}} \end{bmatrix} \begin{bmatrix} \hat{u}_d \\ \hat{u}_q \end{bmatrix} + \begin{bmatrix} 0 \\ -\frac{\Psi_{PMM}}{L_{qM}} \cdot \hat{\omega}_e \end{bmatrix} + \begin{bmatrix} \hat{z}_d \\ \hat{z}_q \end{bmatrix} \tag{4a}$$

$$\frac{d\underline{\hat{i}}_{dq}}{dt} = \underline{A}(\hat{\omega}_e) \cdot \underline{\hat{i}}_{dq} + \underline{B} \cdot \underline{\hat{u}}_{dq} + \underline{N}(\hat{\omega}_e) + \underline{\hat{Z}} \tag{4b}$$

2.3 Error model considering multiple parameter variations

The basis for the application of the hyperstability theory is the transformation of the structure depicted in Fig. 2 into a nonlinear feedback system of the following shape [4].

$$\begin{aligned} \dot{\underline{\delta}} &= \underline{A_E}(\hat{\omega}_e) \cdot \underline{\delta} + \underline{B_E} \cdot \Delta\omega_e = \underline{A_E}(\hat{\omega}_e) \cdot \underline{\delta} - \underline{W_E} = \underline{A_E}(\hat{\omega}_e) \cdot \underline{\delta} + \underline{U_E} \\ \underline{y} &= \underline{\delta} \end{aligned} \tag{5}$$

In the first step, the mathematical transformation into an error model is done subtracting the Eq. (4) describing the adjustable model from the Eq. (2) describing the reference model, shown in Eq. (6).

$$\begin{bmatrix} \delta_d \\ \delta_q \end{bmatrix} = \begin{bmatrix} i_d - \hat{i}_d \\ i_q - \hat{i}_q \end{bmatrix} \tag{6}$$

Decoupling influences of parameter variations from the error model, four further assumptions have to be considered. The connected model parameters in Eq. (4a) should be expressed as shown for example below. A speed error is introduced.

$$\frac{R_{sM}}{L_{dM}} = \frac{R_s}{L_d} + \frac{L_d \cdot \Delta R_s - R_s \cdot \Delta L_d}{L_d \cdot L_{dM}} = \frac{R_s}{L_d} + \Delta\epsilon_{R_d} \tag{7}$$

$$\Delta\omega_e = \omega_e - \hat{\omega}_e \tag{8}$$

$$-\frac{\pi}{2} \le \Delta\epsilon \le \frac{\pi}{2}, cos(\Delta\epsilon) \approx 1 - \frac{(\Delta\epsilon)^2}{2!} + \frac{(\Delta\epsilon)^4}{4!} \tag{9}$$

$$-\frac{\pi}{2} \le \Delta\epsilon \le \frac{\pi}{2}, sin(\Delta\epsilon) \approx \Delta\epsilon - \frac{(\Delta\epsilon)^3}{3!} + \frac{(\Delta\epsilon)^5}{5!} \tag{10}$$

The influence of parameter variations can now be estimated as disturbance and is considered using variable $Z=[z_d\ z_q]^T$. The mathematical description of the error model including influences by uncertainties and tuning parameters is carried out as follows:

$$\begin{bmatrix} \frac{d\delta_d}{dt} \\ \frac{d\delta_q}{dt} \end{bmatrix} = \begin{bmatrix} -\frac{R_s}{L_d} & \hat{\omega}_e \cdot \frac{L_q}{L_d} \\ -\hat{\omega}_e \cdot \frac{L_d}{L_q} & -\frac{R_s}{L_q} \end{bmatrix} \begin{bmatrix} \delta_d \\ \delta_q \end{bmatrix} + \begin{bmatrix} \frac{L_q}{L_d} i_q \\ -\frac{L_d}{L_q} i_d - \frac{\Psi_{PM}}{L_q} \end{bmatrix} (\Delta\omega) + \begin{bmatrix} z_d \\ z_q \end{bmatrix} - \begin{bmatrix} \hat{z}_d \\ \hat{z}_q \end{bmatrix} \tag{11}$$

The disturbance variable $\underline{Z}$ can be further subdivided into different parts, using the following equations.

$$\begin{bmatrix} z_d \\ z_q \end{bmatrix} = \underline{Z} = \underline{Z}_1 + \underline{Z}_2 + \underline{Z}_3 \tag{12}$$

$$\underline{Z}_1 = \begin{bmatrix} -\frac{R_s}{L_d} & \omega_e \cdot \frac{L_q}{L_d} \\ -\omega_e \cdot \frac{L_d}{L_q} & -\frac{R_s}{L_q} \end{bmatrix} \begin{bmatrix} \Delta i_d \\ \Delta i_q \end{bmatrix} - \begin{bmatrix} \frac{d\Delta i_d}{dt} \\ \frac{d\Delta i_q}{dt} \end{bmatrix} + \begin{bmatrix} \frac{1}{L_d} & 0 \\ 0 & \frac{1}{L_q} \end{bmatrix} \begin{bmatrix} u_{dM} - \hat{u}_d \\ u_{qM} - \hat{u}_q \end{bmatrix} \tag{13}$$

$$\underline{Z}_2 = \begin{bmatrix} \Delta\epsilon_{R_d} & -\hat{\omega}_e \cdot \Delta\epsilon_{L_q} \\ \hat{\omega}_e \cdot \Delta\epsilon_{L_d} & \Delta\epsilon_{R_q} \end{bmatrix} \begin{bmatrix} \hat{i}_d \\ \hat{i}_q \end{bmatrix} - \begin{bmatrix} \Delta\epsilon_d & 0 \\ 0 & \Delta\epsilon_q \end{bmatrix} \begin{bmatrix} \hat{u}_d \\ \hat{u}_q \end{bmatrix} - \begin{bmatrix} 0 \\ \Delta\epsilon_{\Psi_{PM}} \end{bmatrix} \cdot \hat{\omega}_e \tag{14}$$

$$\underline{Z}_3 = \begin{bmatrix} \frac{\Psi_{PM}}{L_d} \left(\Delta\epsilon - \frac{(\Delta\epsilon)^3}{3!} + \frac{(\Delta\epsilon)^5}{5!} \right) \\ \frac{\Psi_{PM}}{L_q} \left(\frac{(\Delta\epsilon)^2}{2!} - \frac{(\Delta\epsilon)^4}{4!} \right) \end{bmatrix} \cdot \omega_e - \begin{bmatrix} 2\frac{\Psi_{PM}}{L_d} \left((\Delta\epsilon) - \frac{(\Delta\epsilon)^3}{3!} + \frac{(\Delta\epsilon)^5}{5!} \right) \\ 0 \end{bmatrix} \cdot \hat{\omega}_e \tag{15}$$

Eq. (13) comprises the influence of input and state vector values that are recorded incorrectly, Eq. (14) the effect of parameter variations and Eq. (15) a mix of both.

2.4 Adaptation Mechanism according to Popov's hyperstability

Assuming $\underline{Z} = \hat{\underline{Z}}$, the error model of Eq. (11) could expressed by Eq. (5) to obtain a nonlinear feedback closed-loop system, where the Popov theory can be applied to speed and position determination [4]. At first, it is necessary to prove the eigenvalues of matrix $\underline{A}_E$. The poles have to be located in the left-half complex plane.

$$\underline{H}_E = \left(s\underline{I} - \underline{A}_E(\hat{\omega}_e) \right)^{-1} = \begin{bmatrix} s + \frac{R_s}{L_q} & \hat{\omega}_e \cdot \frac{L_q}{L_d} \\ -\hat{\omega}_e \cdot \frac{L_d}{L_q} & s + \frac{R_s}{L_d} \end{bmatrix} \cdot \frac{1}{\left(s + \frac{R_s}{L_d} \right) \left(s + \frac{R_s}{L_q} \right) + {\hat{\omega}_e}^2} \tag{16}$$

$$Re\left\{ -\frac{R_s \cdot L_q + R_s \cdot L_d}{2 \cdot L_d \cdot L_q} \pm \sqrt{\left(\frac{R_s \cdot L_q + R_s \cdot L_d}{2 \cdot L_d \cdot L_q} \right)^2 - \frac{{R_s}^2}{L_d \cdot L_q} - {\hat{\omega}_e}^2} \right\} \le 0, \tag{17}$$

Eq. (17) is a condition showing that the poles are located in the left-half-plane for the investigated method. Further on, it must be verified that the Popov integral inequality shown below is true for the nonlinear feedback system [6].

$$\forall t_0 > 0, \gamma_0^2 \geq 0, \eta(0,t_0) = \int_0^{t_0} \underline{W_E}^T(\tau)\underline{y}(\tau)\, d\tau \geq -\gamma_0^2 \tag{18a}$$

$$\eta(0,t_0) = \int_0^{t_0} \left[-\frac{L_q}{L_d} i_q(\omega_e - \hat{\omega}_e) \quad \left(\frac{L_d}{L_q} i_d + \frac{\Psi_{PM}}{L_q}\right)(\omega_e - \hat{\omega}_e)\right] \begin{bmatrix}\delta_d \\ \delta_q\end{bmatrix} d\tau \geq -\gamma_0^2 \tag{18b}$$

The adaptive law for the stator frequency could be given in the form of a PI element by Eq. (19) [4], [6].

$$\hat{\omega}_e = K_P \left[\frac{L_q}{L_d} i_q \delta_d - \left(\frac{L_d}{L_q} i_d + \frac{\Psi_{PM}}{L_q}\right)\delta_q\right] + \int_0^{t_0} K_i \left[\frac{L_q}{L_d} i_q \delta_d - \left(\frac{L_d}{L_q} i_d + \frac{\Psi_{PM}}{L_q}\right)\delta_q\right] d\tau \tag{19}$$

2.5 Dynamic response of MRAS-based speed determination

Finding the forward transfer function of the MRAS-based speed determination, the dynamic response of the MRAS-System can be estimated:

$$G_{\omega s}(s) = \underline{c}^T \cdot \underline{H_E} \cdot \underline{b} \tag{20}$$

$$G_{\omega s}(s) = \frac{\left[\frac{L_q}{L_d} i_q \quad \left(-\frac{L_d}{L_q} i_d - \frac{\Psi_{PM}}{L_q}\right)\right]}{\left(s + \frac{R_s}{L_d}\right)\left(s + \frac{R_s}{L_q}\right) + \hat{\omega}_e{}^2} \cdot \begin{bmatrix} s + \frac{R_s}{L_q} & \hat{\omega}_e \cdot \frac{L_q}{L_d} \\ -\hat{\omega}_e \cdot \frac{L_d}{L_q} & s + \frac{R_s}{L_d} \end{bmatrix} \cdot \begin{bmatrix} \frac{L_q}{L_d} i_q \\ \left(-\frac{L_d}{L_q} i_d - \frac{\Psi_{PM}}{L_q}\right) \end{bmatrix} \tag{21}$$

A closed loop block diagram represents the dynamic response of the calculated MRAS-based speed determination and can be described with Eq. (21), shown in Fig. 3. Moreover, its dynamic response is adjustable providing K_p and K_i as defined in Eq. (19).

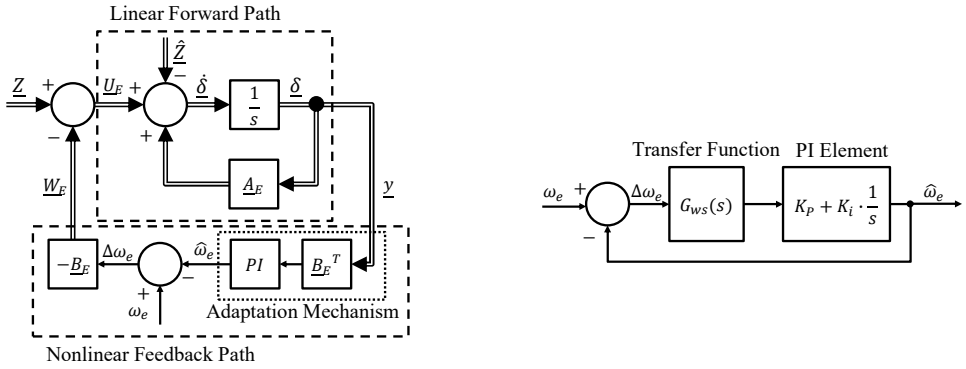

(a) (b)

Fig. 3: MRAS-based closed loop block diagram for speed determination
a) nonlinear and time varying feedback system considering parameter variation
b) block diagram of stator frequency determination

3 Model-based systems engineering approach

In order to compare simulation and experimental results, a model-based systems engineering (MBSE) approach was used, generating software for the µC directly from simulation models. The working procedure applied for this research can be subdivided into four main stages. In the first stage, we used Matlab Simulink 2022a to receive simulation results. Subsequently, in the second stage C-code for the control algorithm was generated by Embedded Coder 7.8 and Embedded Coder Support Package for Texas Instruments C2000 Processors 22.1.1.

On the next stage, the method could be verified using a Rapid Control Prototyping setup with serial communications interface (SCI)-based communication to acquire the data with the sampling time of PWM frequency of 15 kHz. After a functionality check of hardware components, the experimental

verification began. Therefore, a wheel hub drive powered by a five-pole AFPMSM with nominal values P_n=350 W, I_n=10,1 A, M_n=1,11 Nm, n_n=3000 rpm and a gear ratio to the mounted wheel of i=8, was chosen.

3.1 Discrete model implementation

Even if the parameters are exactly defined, model variable deviations occur caused by the implementation. One reason is Euler's method for integration, realised by C code generation e.g. used for sampling operation on microcontrollers [10]. Euler's rule is a typical application to discretize observers for motor drives and also used in this research work. Therefore, the Eq. (4b) and Eq. (19) have to be rewritten into Eq. (22) and Eq. (26). The software code and the sampling operation is executed synchronously to the switching period T_{sw}.

$$\hat{\underline{i}}_{dq}(k+1) = \underline{A}_d(\hat{\omega}_e) \cdot \hat{\underline{i}}_{dq}(k) + \underline{B}_d \cdot \hat{\underline{u}}_{dq}(k) + \underline{N}_d(\hat{\omega}_e) + \hat{\underline{Z}} \tag{22}$$

$$\underline{A}_d(\hat{\omega}_e) = \begin{bmatrix} 1 - T_{sw} \cdot \frac{R_{sM}}{L_{dM}} & \hat{\omega}_e(k) \cdot T_{sw} \cdot \frac{L_{qM}}{L_{dM}} \\ -\hat{\omega}_e(k) \cdot T_{sw} \cdot \frac{L_{dM}}{L_{qM}} & 1 - T_{sw} \cdot \frac{R_{sM}}{L_{qM}} \end{bmatrix} \tag{23}$$

$$\underline{B}_d = \begin{bmatrix} \frac{T_{sw}}{L_{dM}} & 0 \\ 0 & \frac{T_{sw}}{L_{qM}} \end{bmatrix}; \; \underline{N}_d(\hat{\omega}_e) = \begin{bmatrix} 0 \\ -\mathrm{T_{sw}} \cdot \frac{\Psi_{PMM}}{L_q} \cdot \hat{\omega}_e(k) \end{bmatrix}; \; \hat{\underline{Z}} = \begin{bmatrix} \hat{z}_d \\ \hat{z}_q \end{bmatrix} \tag{24}$$

$$fcn(k) = \frac{L_{qM}}{L_{dM}} i_{qM}(k) \delta_{dM}(k) - \left(\frac{L_{dM}}{L_{qM}} i_{dM}(k) + \frac{\Psi_{PMM}}{L_{qM}} \right) \delta_{qM}(k) \tag{25}$$

$$\hat{\omega}_e(k) = \hat{\omega}_e(k-1) + \; K_P \cdot fcn(k) - \; K_P \cdot fcn(k-1) + K_I \cdot fcn(k-1) + \hat{\omega}_e(0) \tag{26}$$

The goal is to compare the simulated and measured results regarding parameter variations. The implemented MRAS-based sensorless control for AFPMSM is depicted in a block scheme in Fig. 4.

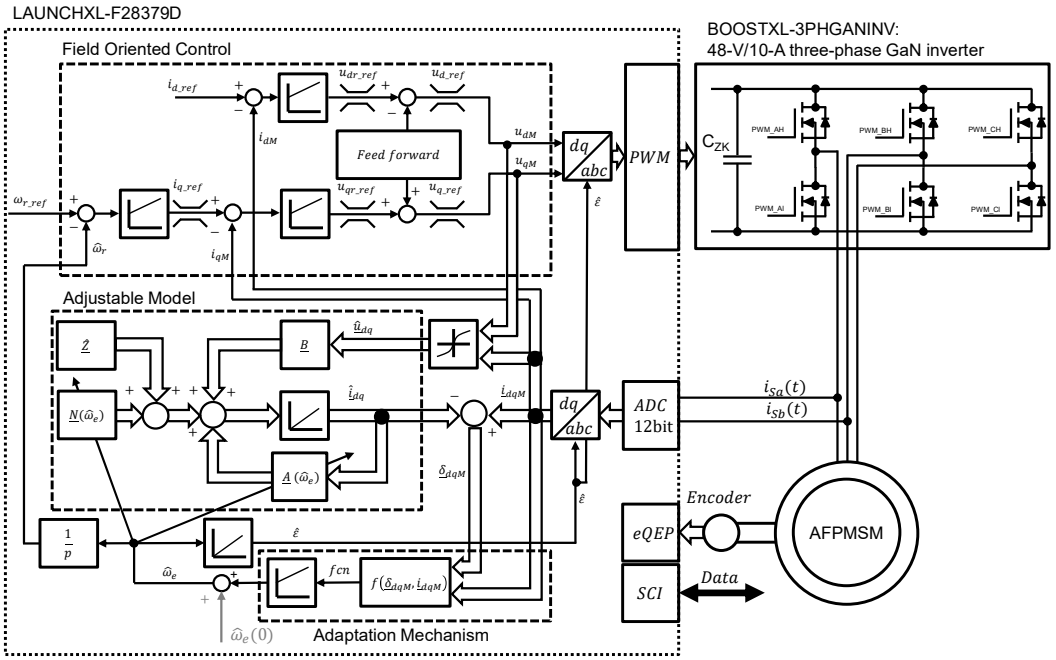

Fig. 4: Block scheme of MRAS-based sensorless control for AFPMSM

4 Simulation and measurement evaluation

Within this paper the sensitivity of parameter uncertainties is illustrated on the basis of the flux orientation angle error. In this way, the impact of parameter variations and measurement errors can be subdivided into static and dynamic disturbance effects, which can be represented by mean value and

standard deviation. Furthermore, the co- and counter-coupling effects of parameter variation in the described error model approach should be assessed by tuning $\underline{\hat{Z}}$.

4.1 Simulation results

Simulation results show the influence of $\underline{\hat{Z}}_d$ and $\underline{\hat{Z}}_q$ interval steps at multi parameter variation. The difference between model and machine parameters was set to $L_{dM}=0{,}85\cdot L_d$, $L_{qM}=1{,}10\cdot L_q$, $R_{sM}=1{,}05\cdot R_s$ and $\Psi_{PMM}=0{,}98\cdot\Psi_{PM}$. Fig. 5 shows the estimated speed, the flux-orientation error for a set reference speed of 1000 rpm depends on interval steps of $\underline{\hat{Z}}$ and electric torque. The parameter set mentioned above led to problems in the implemented MRAS-based sensorless control method with $\underline{\hat{Z}}=0$, presented in Fig. 5 at t=6,8 s. The sensorless startup is implemented without additional methods. This could produce higher torques or overshoots, depending on the initial conditions. Fig. 5 shows that the flux-orientation error can be tuned using $\underline{\hat{Z}}_d$ or $\underline{\hat{Z}}_q$ and is also be tuned at load. Setting $\underline{\hat{Z}}$ to a constant value has only a major effect to the standard deviation of flux-orientation error if the MRAS-based method runs in an unstable point. The mean value of flux-orientation error correlates to $\underline{\hat{Z}}$ presented in Fig. 5.

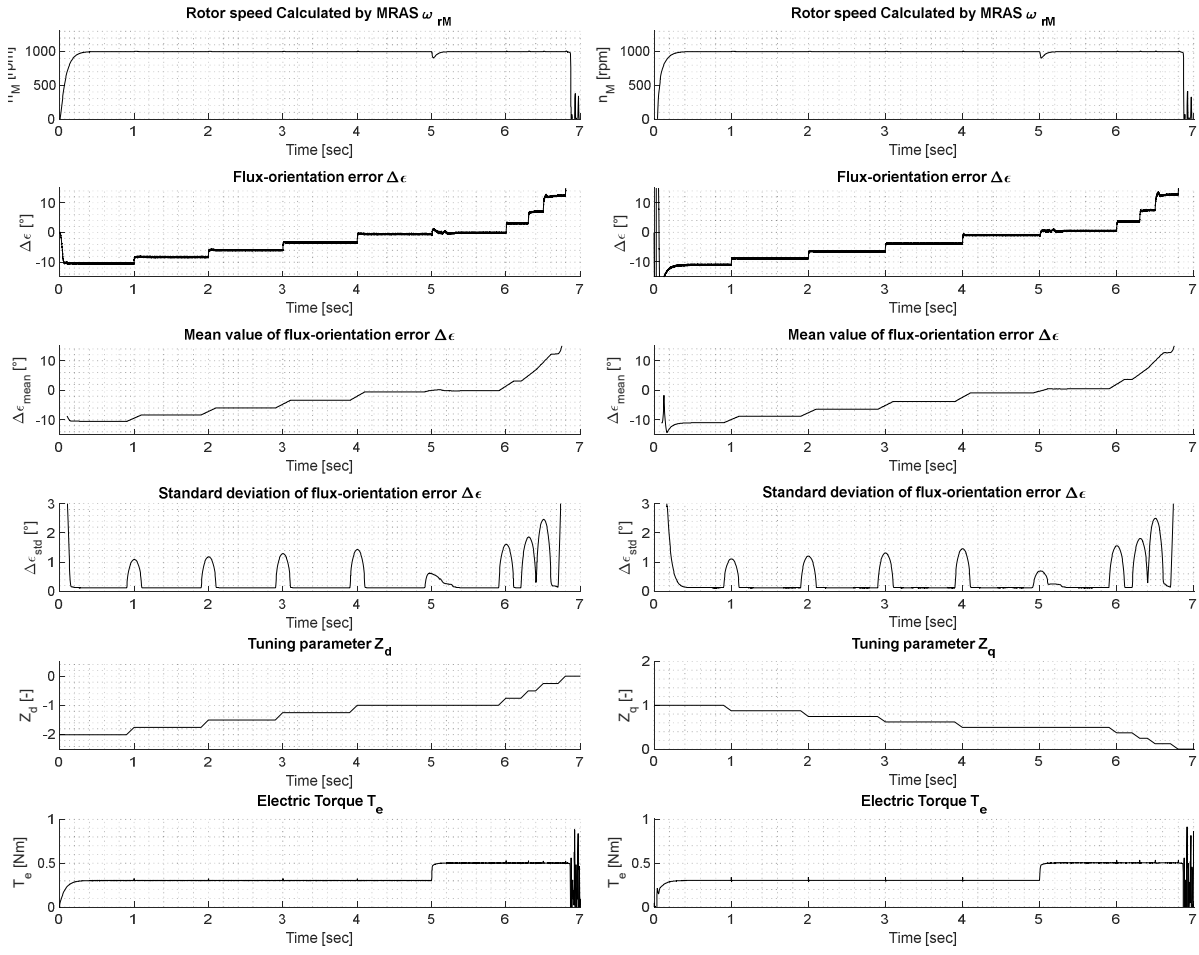

(a) (b)

Fig. 5: Flux orientation error at parameter variations. Stepwise modification of a tuning parameter and load
a) stepwise modification of $\underline{\hat{Z}}_d$ at $\underline{\hat{Z}}_q=0$
b) stepwise modification of $\underline{\hat{Z}}_q$ at $\underline{\hat{Z}}_d=0$

Fig. 6a shows the influence of an implemented noise signal on the measurements of i_{sa} and i_{sb} with a boundary set to ±1 A. Fig. 6b illustrates the effect of an implemented dc-offset measurement error of 0,25 A_{DC} on i_{sa} and i_{sb}. Both have only a minor effect to the mean value of flux-orientation error

compared to Fig. 5. However, the implemented noise signal and dc-offset have more effects on the standard deviation of flux-orientation error and could not be influenced by a constant $\underline{\hat{Z}}$ value.

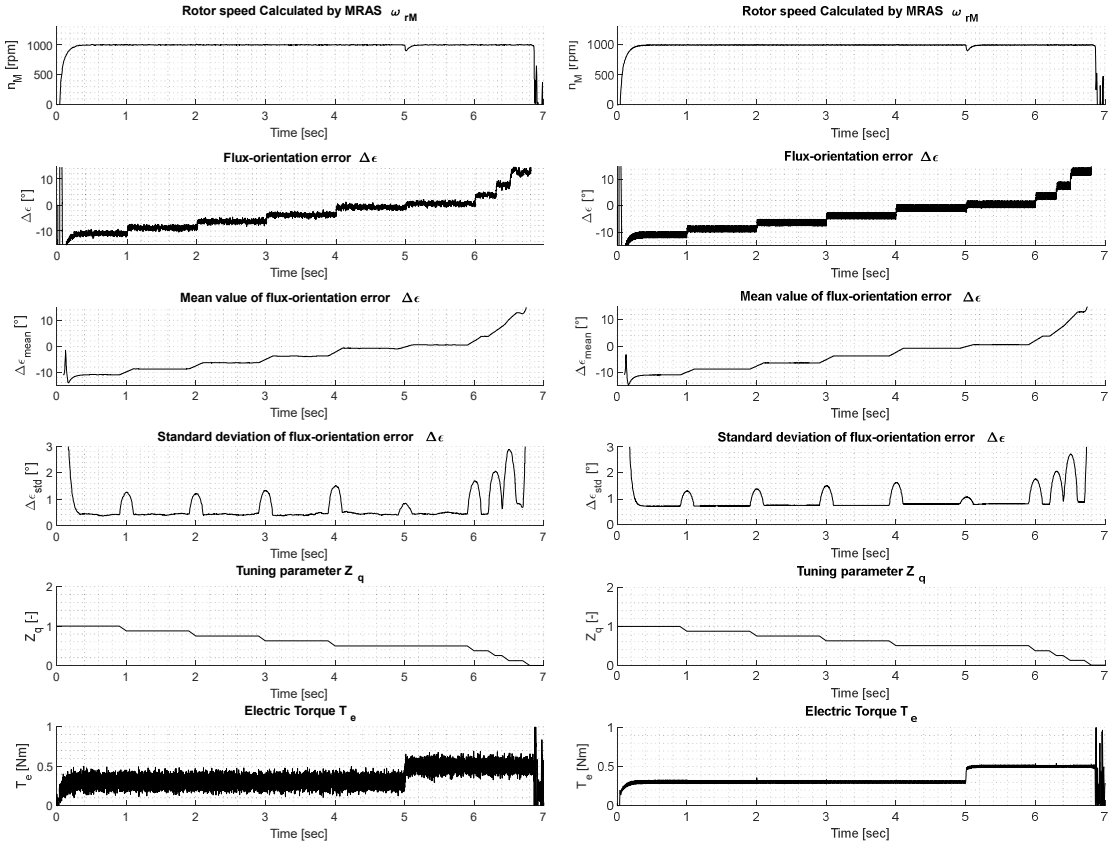

(a) (b)

Fig. 6: Flux orientation error at parameter variations, stepwise modification of $\underline{\hat{Z}}_q$ at $\underline{\hat{Z}}_d$=0 and load
a) implemented current measurement noise
b) implemented current dc-offset

4.2 Measurement results

Measurement results show the influence of $\underline{\hat{Z}}_d$ interval steps at typical parameter variation. The machine parameters were identified by a parameter identification algorithm. The identified parameters are L_d=0,17 mH, L_q=0,17 mH, R_s=0,17 Ω and Ψ_{PMM}=0,0125 Wb. Fig. 5 shows estimated speed, flux-orientation error for a reference speed of 1000 rpm, depending on interval steps of $\underline{\hat{Z}}$ and electric torque. It can be assumed that there is an unknown parameter variation because of the flux orientation error measured at $\underline{\hat{Z}} = 0$, presented in Fig. 7 at t=0 s to 5 s. Furthermore, it can be assumed that there is also an unknown error due to the current measurements, because of the standard deviation of flux orientation error. Moreover, it could be observed a current noise boundary of ±0.6 A at nominal zero current. The sensorless startup is implemented without additional methods. This will produce higher torques or overshoots, depending on the initial conditions. Fig. 7 shows that the flux orientation error can be tuned using $\underline{\hat{Z}}$ and can also be tuned at load. Setting $\underline{\hat{Z}}$ to a constant value has only a major effect to the standard deviation of flux-orientation error if the MRAS-based method runs in an unstable point. The mean value of flux-orientation error correlates to $\underline{\hat{Z}}$ presented in Fig. 7.
Fig. 8 presents the measured flux-oriented angle error by a speed reversal process with and without a tuning parameter $\underline{\hat{Z}}_d$ at $\underline{\hat{Z}}_q$=0. The flux orientation angle can be optimized but has temporary an error peak evoked by reversion.

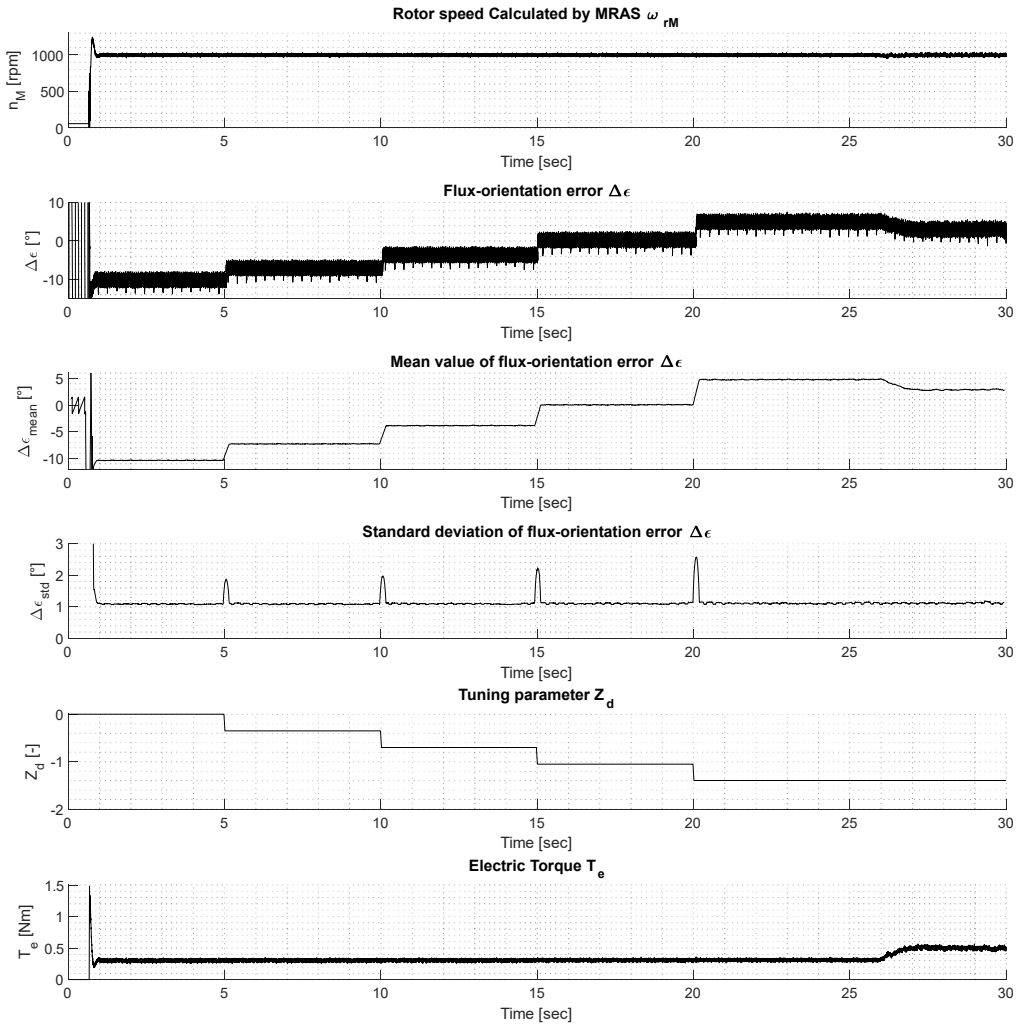

Fig. 7: Measured flux orientation error angle at parameter variations, by stepwise modification of tuning parameter $\underline{\hat{Z}}_d$ at $\underline{\hat{Z}}_q$=0 and load

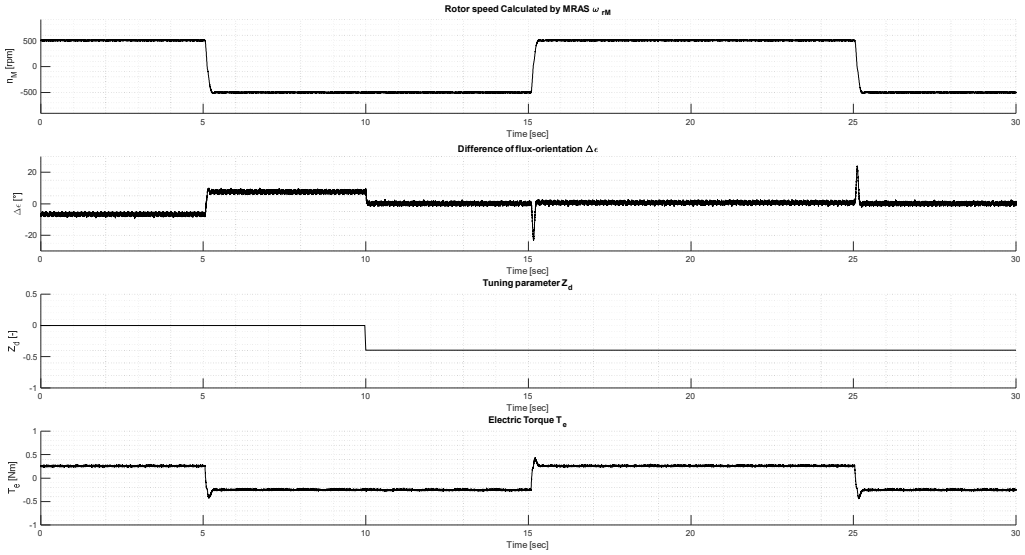

Fig. 8: Measured flux orientation angle error at typical parameter deviations by reversion with and without adapted tuning parameter $\underline{\hat{Z}}_d$ at $\underline{\hat{Z}}_q$=0

5 Conclusion

A MRAS-based sensorless control strategy designed for medium and high stator frequencies was investigated on a wheel hub drive with an AFPMSM in dependence of parameter sensitivity.
In a first step, the sensorless control method was introduced. Effects of multiple parameter variations and incorrectly recorded input and state vector values were described by a mathematical model. Dynamic response was also calculated. By enhancing the fundamental wave model with a tuning parameter, the effects of multiple parameter variations could be partially balanced. Furthermore, the sensorless method was simulated with an MBSE approach to be subsequently implemented on a target system.
By using the mean value and standard deviation of flux orientation error it could be shown that parameter variations have static and dynamic effects on the accuracy of the control. Setting the tuning parameter to a fixed value, the static effects could be reduced or increased. Thus, unstable operating points, that result from parameter variation, can be handled by well-chosen tuning parameters.
From simulation results it could be observed that a current measurement error has dynamic effects on the flux orientation error. This was shown using DC and noise signal offsets. The proposed sensorless control method works on a microcontroller, common in industrial applications.

References

[1] A. Cavagnino, M. Lazzari, F. Profumo, und A. Tenconi, „A comparison between the axial flux and the radial flux structures for PM synchronous motors“, *IEEE Trans. Ind. Appl.*, Bd. 38, Nr. 6, S. 1517–1524, Nov. 2002, doi: 10.1109/TIA.2002.805572.

[2] K. Sitapati und R. Krishnan, „Performance comparisons of radial and axial field, permanent-magnet, brushless machines“, *IEEE Trans. Ind. Appl.*, Bd. 37, Nr. 5, S. 1219–1226, Sep. 2001, doi: 10.1109/28.952495.

[3] G. Wang, M. Valla, und J. Solsona, „Position Sensorless Permanent Magnet Synchronous Machine Drives—A Review“, *IEEE Trans. Ind. Electron.*, Bd. 67, Nr. 7, S. 5830–5842, Juli 2020, doi: 10.1109/TIE.2019.2955409.

[4] A. Khlaief, M. Boussak, und A. Châari, „A MRAS-based stator resistance and speed estimation for sensorless vector controlled IPMSM drive“, *Electr. Power Syst. Res.*, Bd. 108, S. 1–15, März 2014, doi: 10.1016/j.epsr.2013.09.018.

[5] X. Liu, G. Zhang, L. Mei, und D. Wang, „Speed estimation and Parameters Identification simultaneously of PMSM based on MRAS“, Bd. 12, S. 10, 2017.

[6] J. Zhao, X. Zhang, C. Lin, und G. Tian, „Simulation research of sensorless control of PMSM based on MRAS considering parameters variation and dead-time“, in *2016 19th International Conference on Electrical Machines and Systems (ICEMS)*, Nov. 2016, S. 1–6.

[7] Y. Ni und D. Shao, „Research of Improved MRAS Based Sensorless Control of Permanent Magnet Synchronous Motor Considering Parameter Sensitivity“, in *2021 IEEE 4th Advanced Information Management, Communicates, Electronic and Automation Control Conference (IMCEC)*, Juni 2021, Bd. 4, S. 633–638. doi: 10.1109/IMCEC51613.2021.9482131.

[8] K. Liu, Q. Zhang, Z.-Q. Zhu, J. Zhang, A.-W. Shen, und P. Stewart, „Comparison of two novel MRAS based strategies for identifying parameters in permanent magnet synchronous motors“, *Int. J. Autom. Comput.*, Bd. 7, Nr. 4, S. 516–524, Nov. 2010, doi: 10.1007/s11633-010-0535-3.

[9] N. P. Quang und J.-A. Dittrich, *Vector Control of Three-Phase AC Machines*, Second Edition. Springer-Verlag Berlin Heidelberg, 2015. [Online]. Verfügbar unter: https://link.springer.com/book/10.1007/978-3-662-46915-6

[10] M. Comanescu, „Influence of the discretization method on the integration accuracy of observers with continuous feedback“, in *2011 IEEE International Symposium on Industrial Electronics*, Juni 2011, S. 625–630. doi: 10.1109/ISIE.2011.5984230.

[11] B. Saunders, G. Heins, und F. De Boer, „Framework for sensitivity analysis of industry algorithms for sensorless PMSM drives“, in *AUPEC 2011*, Sep. 2011, S. 1–6.